

Cite this: *Nanoscale*, 2018, **10**, 733

Efficient skyrmion transport mediated by a voltage controlled magnetic anisotropy gradient†

Xuan Wang,[†] W. L. Gan,[‡] J. C. Martinez,^c F. N. Tan,^a M. B. A. Jalil^c and W. S. Lew^{*a}

Despite the inefficiencies associated with current-induced spin torques, they remain the predominant mode of skyrmion propulsion. In this work, we demonstrate numerically that skyrmions can be transported much more efficiently with a voltage-controlled magnetic anisotropy (VCMA) gradient. An analytical model was developed to understand the underlying skyrmion dynamics on a track under the VCMA conditions. Our calculations reveal that the repulsive skyrmion-edge interaction not only prevents the skyrmion from annihilating but also generates most of the skyrmion propulsion. A multiplexed array of gate electrodes can be used to create discrete anisotropy gradients over a long distance, leading to the formation of a series of translatable skyrmion potential wells. Due to the strong confining potentials, skyrmions are transported at a 70% higher packing density. Finally, we demonstrated that this form of skyrmion propulsion can also be implemented on almost any 2D geometry, providing improved versatility over current-induced methods.

Received 31st August 2017,
Accepted 29th November 2017

DOI: 10.1039/c7nr06482a

rsc.li/nanoscale

Introduction

Magnetic skyrmions are topologically non-trivial spin textures with diameters in the nanometer length scale. Despite their small sizes, they are stable against moderate perturbations with the support of interfacial Dzyaloshinskii–Moriya interactions (DMI) originating from ultrathin films exhibiting high spin–orbit coupling.^{1–3} As a result, these topological objects show great promise for use in next generation ultra-high density non-volatile memory devices.^{4,5} To realize such devices, much of the current research on skyrmion dynamics is focused on skyrmion transport *via* the application of spin-polarized currents.^{6–10} However, though applying high current densities on the order of 10^{11} A m⁻² enables high-speed manipulation of skyrmion motions it also leads to skyrmion stability issues.^{8,11–14} Under such high current densities, Joule heating significantly increases the device temperature, further

leading to device instability. Besides the increased risk of skyrmion annihilation due to a higher thermal field, studies by Sug-Bong Choe *et al.* and A. Yamaguchi *et al.* have also shown that temperature can have a strong influence on the propagation speeds of magnetization textures.^{15–17} Therefore, it is necessary to develop an energy efficient skyrmion manipulation technique that reduces the Joule heating.

To increase efficiency in magnetic devices, many recent scientific endeavors have focused on the study of voltage-controlled magnetic anisotropy (VCMA). The effect relies on the electric field-induced change in the relative occupation of 3d orbitals to alter the magnetic anisotropy.^{18–22} Since VCMA is a field-induced effect, it consumes much lower energy as compared to the electric current-based methods. By applying a gate voltage across an insulating layer, the magnetic anisotropy of the ferromagnetic layer can be modulated. The VCMA effect has already been shown to be large enough for magnetization switching in magnetic random-access memory devices and for speeding up domain wall transport.^{23–31}

In this work, we demonstrate that skyrmions can be efficiently driven by a gradient in the voltage-controlled magnetic anisotropy. A model has been developed that can accurately predict the skyrmion speed and trajectory under different anisotropy gradients. From the model, we found that the edge repulsion is not only responsible for preventing skyrmion annihilation at the edges, but it also provides most of the propulsive force in skyrmion driving. Therefore, edge engineering will greatly improve the performance of anisotropy gradient-driven skyrmion devices.^{8,11,32} To apply a significant

^aSchool of Physical and Mathematical Sciences, Nanyang Technological University, 21 Nanyang Link, Singapore 637371. E-mail: wensiang@ntu.edu.sg

^bDepartment of Physics, School of Science, Lanzhou University of Technology, Lanzhou 730050, People's Republic of China. E-mail: wangxuan2010@lut.cn

^cElectrical and Computer Engineering Department, National University of Singapore, 4 Engineering Drive 3, Singapore 117576

† Electronic supplementary information (ESI) available: Calculation of the dissipative force tensor D , calculation of the coefficient $C(x)$ in the equation of F_y , movie of skyrmion motion under continuous anisotropy gradient in a strip nanowire, movie of skyrmion motion under stepped anisotropy in a racetrack. See DOI: 10.1039/c7nr06482a

‡ First authors.

anisotropy gradient over large distances, a multiplexed array of discrete gate electrodes was used to modulate the magnetic anisotropy. In this scheme, an array of skyrmion potential wells is created which trap the skyrmions and when moved, conveniently transports the skyrmions.

Results and discussion

Skyrmion dynamics under a VCMA gradient in an infinite plane

We first consider the motion of a skyrmion on an unconfined planar skyrmion system under the influence of a magnetic anisotropy gradient. To model the infinite system, periodic boundary conditions were imposed on both x -axis and y -axis that enables the magnetization to wrap around in both directions and a Néel skyrmion typical of systems with interfacial DMI was used as the starting configuration.^{33,34} The VCMA gradient across the wedged insulating layer was modelled by a gradient in the magnetic anisotropy energy density of $\frac{dK_u}{dx} = 600 \text{ GJ m}^{-4}$ along the x -axis, and controlled by the application of an electric field along the z -axis *via* gates, as shown in Fig. 1(a). This corresponds to a percentage change of 7.5% over a length of $1 \mu\text{m}$. Upon the application of an anisotropy gradient, the skyrmion was observed to propagate in a single direction indefinitely.

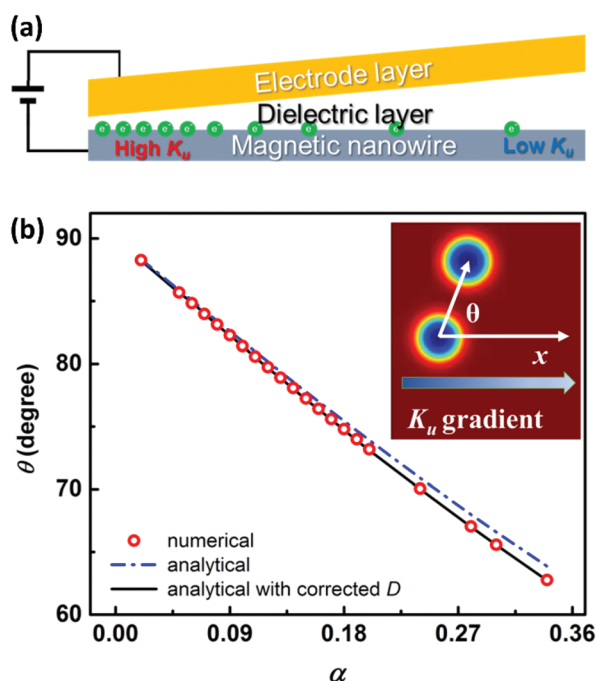


Fig. 1 (a) Schematic of a voltage controlled magnetic anisotropy device capable of creating an anisotropy gradient. (b) The deviation angle θ of skyrmion motion to the direction of the K_u gradient $\frac{dK_u}{dx} = 600 \text{ GJ m}^{-4}$ as a function of the Gilbert damping constant α in a wide plane, in which the skyrmion moves at an angle θ with respect to the x -axis. The inset is a snapshot of a skyrmion, which drifted diagonally after a K_u gradient was applied.

Assuming that the skyrmion magnetization profile performs a translation without deformation, the isolated Néel skyrmion can be considered as a rigid point-like particle. The skyrmion dynamics can then be modeled within the framework of the Thiele equation without polarized spin current given by,^{7,35,36}

$$G\hat{z} \times \vec{v} - D\alpha\vec{v} + \frac{\gamma}{M_s d} \vec{F} = 0 \quad (1)$$

$$\vec{G} = 2\pi[\cos\theta]_{\theta(r=0)}^{\theta(r=\infty)} \hat{z} \quad (2)$$

$$\vec{F} = - \int_{\text{UC}} d^2r \partial \vec{n} \cdot \frac{\delta E}{\delta \vec{n}} \quad (3)$$

where v is the skyrmion drift velocity, G is the gyromagnetic coupling vector that depends on the direction of the magnetization in the skyrmion core and far away from the core, D is the dissipative force tensor that is dependent on the radial profile of the out-of-plane angle of the skyrmion, and α is the Gilbert damping constant. The vector F is a force acting on the skyrmion, originating from an inhomogeneous magnetostatic energy landscape.

The first term of the Thiele equation describes the gyrotropic motion of a skyrmion,^{6,37–39} which gives rise to a Hall-like behavior of magnetic skyrmions (SkHE)⁴⁰ which causes them to deviate from the direction of the applied stimulus as shown in Fig. 1(b) inset. The second term is the dissipative force originating from the Gilbert damping while the third term is the driving force originating from the inhomogeneous energy landscape which is attributed to the magnetic anisotropy gradient. To simplify the Thiele equation, the skyrmion motion is decomposed into the x -component and the y -component:

$$\hat{x} : Gv_y + D\alpha v_x = \frac{\gamma}{M_s d} F_x \quad (4)$$

$$\hat{y} : Gv_x - D\alpha v_y = 0 \quad (5)$$

which leads to the expression for the ratio of v_y and v_x :

$$\tan\theta = \frac{v_y}{v_x} = \frac{G}{\alpha D} \quad (6)$$

For a Néel-type skyrmion with $\alpha = 0.1$, the calculated skyrmion Hall angle θ of 82° results in mostly transverse motion. Micromagnetic simulations were performed to verify the dependence of the skyrmion Hall angle on α . Indeed, a linear relation shown in Fig. 1(b) was observed as predicted. However, a discrepancy between the numerical results and the analytical expression (eqn (6)) exists which increases with α . This difference can be almost completely accounted for by the change of the skyrmion magnetization profile as the skyrmion moves from a region of higher K_u to a region of lower K_u . The resulting change in D can be calculated by numerically integrating the volume magnetization (see the ESI †). The inset of Fig. 1(b) shows the relation between the modified D and α . By introducing this modified D back into eqn (6), the theoretical results now match almost exactly the simulation results.

Therefore, we have shown that the skyrmion Hall angle is determined by α even in the absence of a spin current.

VCMA gradient-induced skyrmion dynamics in finite systems

Translation invariance on an infinite plane is commonly invoked to argue that a skyrmion velocity is not a function of its position. However, a skyrmion on a finite track is no longer translationally invariant. Therefore, the energy potential from the edges must be considered in a finite system. Over a large range of nanowire width values, the skyrmion is observed to drift towards the edges with an angle of 82° but starts to travel parallel to the edge close to its vicinity and does not annihilate, as shown in Fig. 2(a). The dependence of trajectory on nanowire width, as shown in Fig. 2(b), implies that repulsive potential plays a key role to repel a skyrmion from the edges.^{41,42}

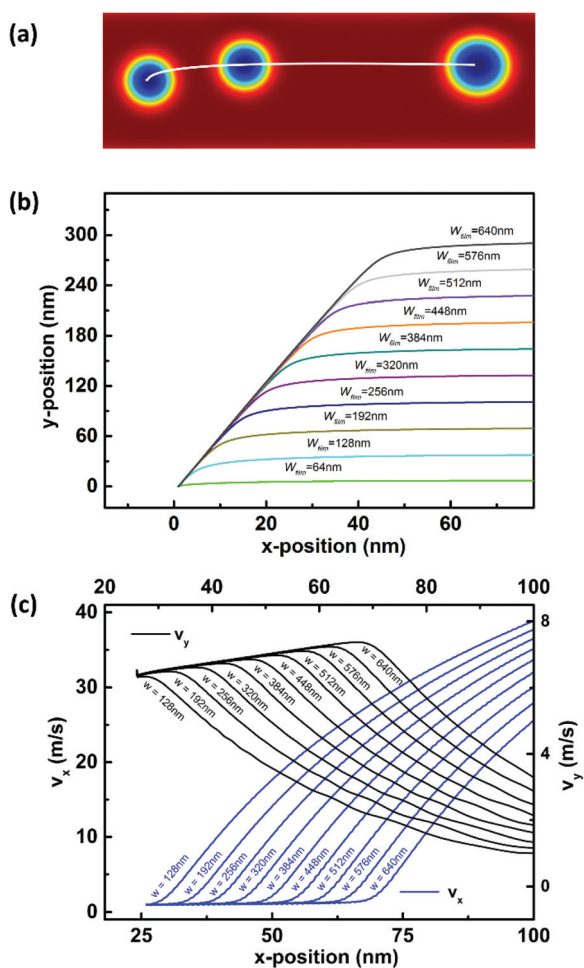


Fig. 2 Skyrmion motion in a nanowire induced by an anisotropy energy gradient along the x-axis. (a) Snapshots of a skyrmion motion at 2 ns intervals in a 64 nm wide nanowire. (b) Skyrmion trajectories in nanowires of different widths, from 64 nm to 640 nm, indicating that the skyrmion trajectory is highly dependent on nanowire geometry. (c) The longitudinal and transverse velocities (v_x , v_y), at the different nanowire widths. v_y slows down to almost zero at the end of its displacement along the y-axis; meanwhile, v_x dramatically increases from several m s^{-1} to tens of m s^{-1} .

As the skyrmion approaches the edges, its motion soon becomes parallel to the nanowire (see the ESI 4†). This leads us to the conclusion that \vec{F} in eqn (1) must include the repulsive potential if the system is finite. The Thiele equation can be rearranged to express velocity \vec{v} as:

$$\vec{v} = \frac{\gamma}{(G^2 + D^2\alpha^2)M_s d} (D\alpha\vec{F} + (\vec{G} \times \vec{F})) \quad (7)$$

As discussed before, \vec{F}_x originates from the inhomogeneous energy attributable to the K_u gradient which can be written as,

$$F_x = \frac{dE_{K_u}}{dK_u} \frac{dK_u}{dx} \quad (8)$$

$$E_{K_u} = -K_u(\vec{m} \cdot \hat{z})^2 \pi R_{sk}^2 d \quad (9)$$

Here E_{K_u} is the anisotropy energy,⁴³ d is the thickness of the skyrmion system, and R_{sk} is the radius of the skyrmion. Eqn (9) predicts that the decrease of K_u leads to the decrease of energy in the skyrmion system, which is consistent with the observation that skyrmions tend to move to a region of lower K_u . From the above, we can also see that a larger anisotropy gradient will create a larger driving force which in turn leads to a higher speed, a trend confirmed by numerical results, as shown in Fig. 3(a).

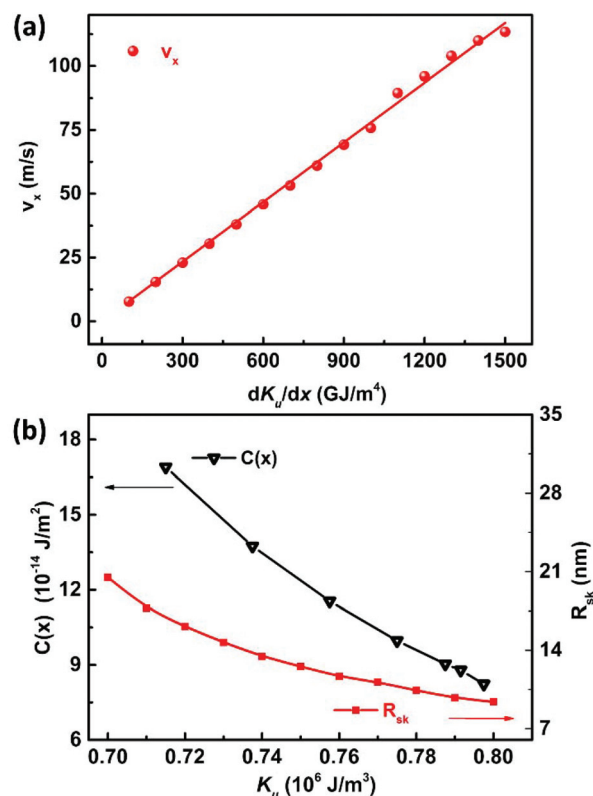


Fig. 3 (a) Numerically calculated values of saturation velocities $v_{x,T}$ vs. $\frac{dK_u}{dx}$, indicating that v_x is directly proportional to $\frac{dK_u}{dx}$. (b) Total energy gradient of a skyrmion along the y-axis as a function of the anisotropy constant.

In the case of a finite nanowire system, the repulsive potential exists in the edge of the skyrmion system which leads to a force pushing the skyrmion back to the center position. At the center, where y displacement from the center of the nanowire (Δy) is zero, this force is also zero as expected from the symmetry along the x -axis. However, when the skyrmion is displaced towards the top or bottom edge ($\Delta y \neq 0$), an increased magnetostatic energy creates a repulsive potential from the edges, keeping the skyrmion from approaching the edges.^{41,42,44} The force originates from the repulsive potential for a nanowire of width w and can then be expressed by,

$$F_y = \frac{\partial E_y}{\partial y} = C(x)\Delta y, \quad \frac{w}{2} - |\Delta y| \geq 20 \text{ nm} \quad (10)$$

Here, $C(x)$ is the magnetostatic interaction coefficient. As F_y is assumed to be purely magnetostatic in nature, the linear relation proposed is only valid for a small region about the center of the nanowire (see ESI 2†). When the skyrmion center is less than 20 nm from the edge, a strong attractive potential is experienced which can cause skyrmion annihilation (see ESI 5†). The coefficient C was also found to have a dependence on the x -position which suggests a dependence on the effective K_u experienced by the skyrmion; since the skyrmion is magnetically charged, a larger skyrmion experiences a larger repulsion from the edges. To obtain the function $C(x)$, the gradient of energy *versus* Δy was extracted from numerically calculated data. As expected, C decreases with increasing K_u as shown in Fig. 3(b).

In our analysis thus far, we have established that the skyrmion propulsion induced by the anisotropy energy gradient is determined by the interplay between two forces, the first of which is a driving force which causes the skyrmion to move along the x -axis, and originates from the anisotropy energy gradient. Secondly, there is a repulsive force denoted by the inhomogeneous magnetostatic energy landscape perpendicular to the edge (see ESI 2†). By combining the two forces, we can generate a two-dimensional force (F_x, F_y) vector field in the x - y plane, as shown in Fig. 4(a). In a system without SkHE, a skyrmion will move in the $+x$ direction monotonically while the edge interaction forms a potential well keeping the skyrmion at the center of the nanowire. The situation becomes interesting when a force field is transformed into a velocity field by applying eqn (7). While the force field is symmetric along the x -axis, the SkHE destroys the symmetry in the velocity field. As shown in Fig. 4(b), the system is asymmetric and the equilibrium trajectory is shifted upwards. In this context, the equilibrium trajectory is defined as the trajectory at which the skyrmion moves in the direction along the nanowire; all other y -displacements will result in the skyrmion returning to the equilibrium trajectory.

An important consequence of the asymmetry is that the initial skyrmion position can significantly modify the skyrmion trajectory. As shown in Fig. 4(c), it is possible for the skyrmion to perform a boomerang maneuver whenever it is nucleated closer to the bottom edge. This phenomenon results from the strong repulsive potential overpowering the forward

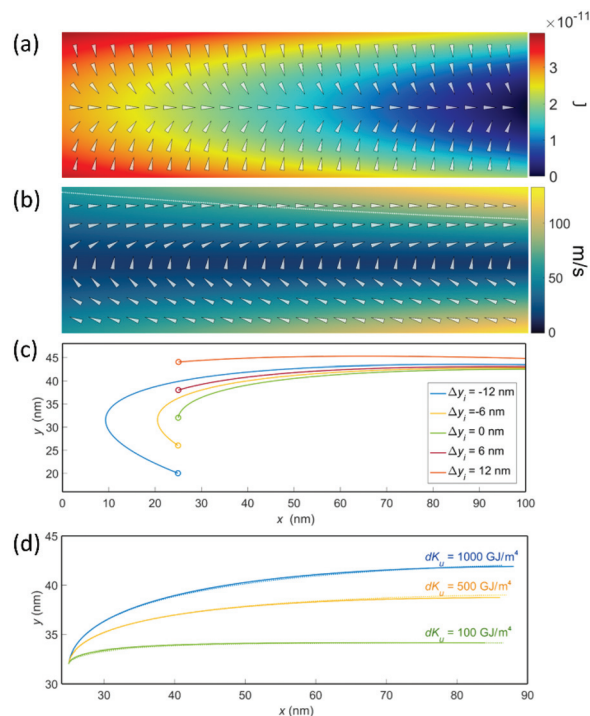


Fig. 4 (a) 2D force field of the system as a function of skyrmion position on the nanowire (100 nm × 64 nm). (b) 2D skyrmion velocity field. The equilibrium trajectory is marked by the white dotted lines. (c) The trajectories of skyrmion motion with different initial (Δy) obtained by evolving eqn (8) in small time steps. (d) Skyrmion trajectory calculated from micromagnetic simulations (solid line) and analytically (dotted).

propulsion, resulting in an initial backward motion. As the skyrmion passes the center of the nanowire ($\Delta y = 0$ nm), the edge interaction changes in sign and propels the skyrmion forward instead, thus completing the boomeranged maneuver. However, the trajectories of skyrmions at all initial positions still converge towards the equilibrium trajectory. In the equilibrium trajectory, the terminal x -velocity can be expressed as,

$$v_{xT} = \frac{\gamma}{M_s d} \frac{F(x)}{D\alpha} = \frac{\gamma \pi m_z^2 R_{sk}^2}{M_s D \alpha} \frac{dK_u}{dx}. \quad (11)$$

Eqn (11) assumes that the repulsive edge potentials are sufficient to prevent the skyrmion from annihilation and shows that the terminal velocity of a skyrmion is proportional to $\frac{dK_u}{dx}$, consistent with the numerical result shown in Fig. 3(a). This equation also highlights how the material parameters such as D , α and M_s can affect the velocity of skyrmion motion. Meanwhile, the y -displacement at which terminal velocity is achieved can be expressed analytically as,

$$\Delta y_T = \frac{\pi R_{sk}^2 m_z^2 G d}{C(x) D \alpha} \frac{dK_u}{dx}. \quad (12)$$

It is trivial to see from eqn (12) that with a higher $\frac{dK_u}{dx}$, the equilibrium trajectory gets shifted upwards. However, eqn (12) also reveals that the maximum velocity is in fact limited by the

edge interaction. For a finite system, $\Delta y_T \leq \left(\frac{w}{2} - 20 \text{ nm}\right)$ determines the maximum force along the y -axis; skyrmion annihilation would occur readily when the skyrmion center is less than 20 nm from the edge (see ESI 5[†]). A dilemma results, in which a larger anisotropy gradient will increase the skyrmion transport velocity but once the maximum F_y is exceeded, skyrmion annihilation will result.

Stepped anisotropy gradient for skyrmion transport on a curved track

To increase the skyrmion velocity, a larger anisotropy gradient is favored. However, for a skyrmion to remain stable, the K_u should be kept above $0.56 \times 10^6 \text{ J m}^{-3}$. This leads to a limitation that fast moving skyrmions can only exist in relatively short nanowires. To allow for devices of any arbitrary length, we propose the use of discrete gate electrodes instead of a single gate electrode that covers the entire device. In such a scheme, an anisotropy gradient can be created when adjacent parts of the nanowire have different K_u values.

Fig. 5(a) shows the schematic of such a device. The device uses a repeated array of three gate electrodes which can modulate the magnetic anisotropy of the adjoining track region to be one of the three states; +2.5% (high), -2.5% (low) or

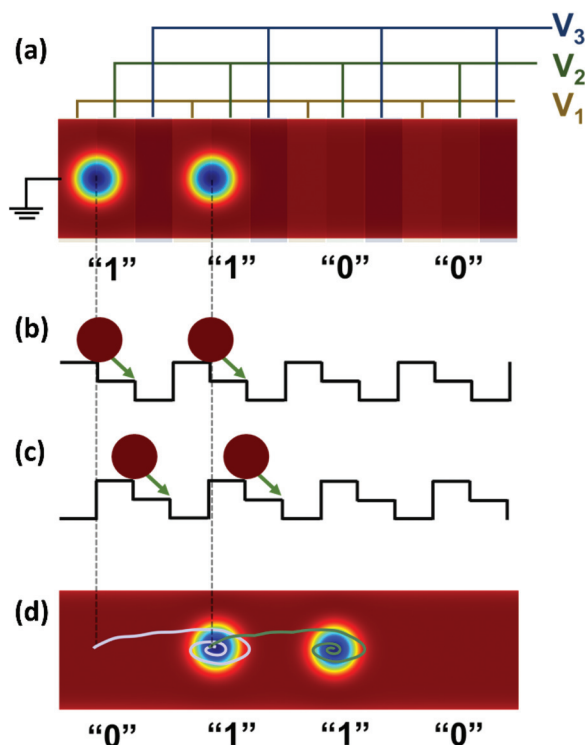


Fig. 5 (a) Schematic diagram of a multiplexed gate architecture for controlling the anisotropy gradient. (b) Magnetostatic energy levels across the length of the nanowire demonstrating how the stepped voltages can create potential wells. The potential gradient-induced motion of the skyrmion is indicated by the green arrows. (c) Magnetostatic energy levels after a “shift” operation. (d) Magnetization snapshot after three consequent shift operations.

unchanged (off). Therefore, when the states of three consecutive electrodes are set to off–low–high, a potential well is formed at the second electrode. The electrodes in each set of three electrodes are also multiplexed; since each electrode is connected to its next nearest neighbor, a series of skyrmion potential wells are formed as shown in Fig. 5(b and c). In this way, the skyrmion–skyrmion repulsion can be overcome and the spacing between the skyrmions can be kept constant. For conventional skyrmion-based devices, the skyrmions should have a spacing of at least 2.6 times larger than their diameter to minimize the skyrmion–skyrmion interaction.⁴⁵ In our device, skyrmions are packed at 1.5 times their diameter, which increases the packing density by at least 70%. The strong confining potentials also trap skyrmions in discrete positions without the need for inefficient geometrical pinning sites.¹¹

To propel the skyrmion, the electrode voltages are then changed to the low–high–off states, which shift the potential well to the right. In the device, the use of three electrodes allows us to ensure that skyrmions are always propelled in one direction; in a device with groups of only two electrodes, a skyrmion sitting at a high state electrode has the equal likelihood to shift in either direction as both the adjacent electrodes would have the same potential. The shift operation can be repeated indefinitely and with a change in K_u between the gates at $\pm 2.5\%$, an average velocity of 70 m s^{-1} was achieved. Increasing the change in K_u to above $\pm 2.5\%$ leads to eventual annihilation at the edge. The change of K_u at $\pm 2.5\%$ between the gates correlates to a $\frac{dK_u}{dx}$ of 1300 GJ m^{-4} , which should produce a skyrmion velocity of 102.8 m s^{-1} according to eqn (11). However, as only a part of the skyrmion is on the anisotropy step at any given time, the effective $\frac{dK_u}{dx}$ acting on the skyrmion is decreased, unlike in a smooth K_u gradient which eqn (11) is based on.

To quantify the power consumption for skyrmion transport, the power cost of transporting a single skyrmion at 1 ms^{-1} is calculated. Using this metric, skyrmion transport in our VCMA device is estimated to cost 9 pW ms^{-1} , while the current-driven skyrmion transport systems typically require 7 nW ms^{-1} (see ESI 3[†]).

Besides the improved energy efficiency, the use of discrete gate electrodes allows anisotropy gradient-induced skyrmion transport to be implemented on almost any arbitrary 2D geometries. Of interest is a closed loop structure which allows skyrmion read/write operations to be non-destructive (see ESI 6[†]). In contrast, conventional nanotrack devices must be at least twice as long as the skyrmion chain in order for the entire skyrmion chain to traverse past the central read–write heads. In other words, at least half the nanowire must be used as a skyrmion buffer for reading. As shown in Fig. 6, the use of a closed loop enables skyrmions to be returned to their original positions after read/write, thus removing the need for a skyrmion buffer area. The ability to continuously shift the entire skyrmion chain by applying the same excitation can also simplify the design of skyrmion devices.

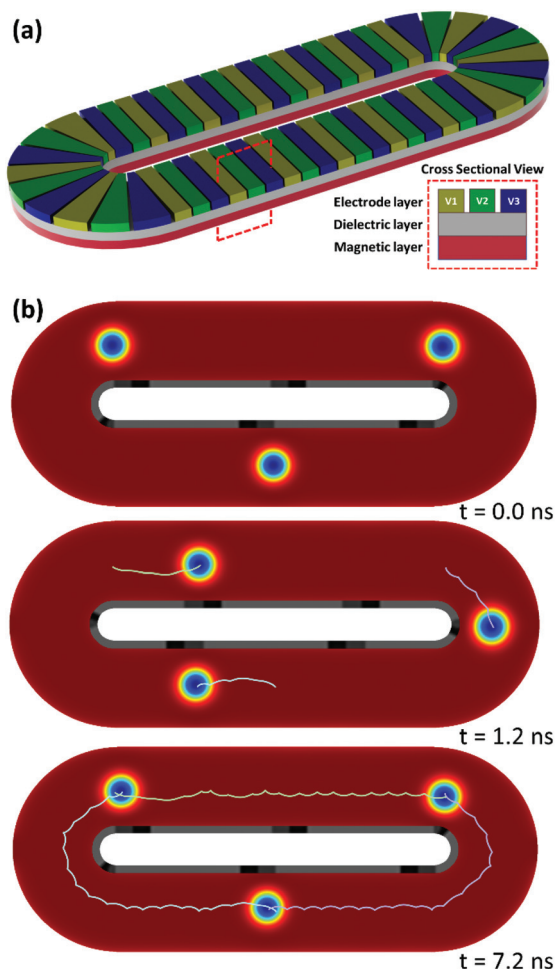


Fig. 6 (a) 3D schematic diagram of a stepped anisotropy for racetrack memory. The electrode layer V_1 , V_2 and V_3 corresponds to those in Fig. 5. (b) Snapshots of skyrmions' instantaneous positions at $t = 0$ ns, $t = 1.2$ ns and $t = 7.2$ ns, respectively. There are 3 skyrmions in the system and 6 sets of K_u , which are represented by the gray rectangle in the center loop and induced by a voltage gate. When the gate voltage is switching clockwise, skyrmions are driven clockwise.

Conclusions

In conclusion, we have shown that skyrmions can be driven by an anisotropy gradient created *via* applying a gate voltage in the absence of spin current. A model was developed to understand the forces acting on a skyrmion under an anisotropy gradient. Using the model, the skyrmion's speed and trajectory can be accurately predicted. To create anisotropy gradients of any arbitrary length without a large variation in anisotropy, an alternative scheme of using the stepped magnetic anisotropy was demonstrated. As compared to conventional spin torque-driven skyrmion devices, the use of discrete anisotropy steps in both a nanowire and a closed loop geometry is not only three orders more energy efficient but also greatly increases skyrmion packing density. Our work here provides insights into the development of anisotropy gradient-driven skyrmion devices and paves the way for their realization.

Calculation methods

The micromagnetic simulations are performed using MuMax3.⁴⁶ The time-dependent magnetization dynamics is expressed by using the modified Landau-Lifshitz-Gilbert (LLG) equation,^{47,48}

$$\frac{d\vec{M}}{dt} = -\gamma\vec{H}_{\text{eff}} \times \vec{M} + \frac{\alpha}{M_s}\vec{M} \times \frac{d\vec{M}}{dt} \quad (13)$$

Here, γ is the Gilbert gyromagnetic ratio, α is the Gilbert damping coefficient and \vec{M} is the magnetization. H_{eff} is the effective field acting on the local magnetization which includes the symmetric exchange interaction with exchange stiffness A , perpendicular anisotropy, magnetostatic interaction and interfacial DMI. For micromagnetic simulations, a discretization of $1 \text{ nm} \times 1 \text{ nm} \times 0.5 \text{ nm}$ is used which is sufficiently smaller than the exchange length and the skyrmion size. The experimentally obtained material parameters of Pt/Co were used for the simulations: saturation magnetization $M_s = 6 \times 10^5 \text{ A m}^{-1}$, exchange stiffness $A = 13 \times 10^{-12} \text{ J m}^{-2}$, DMI constant D fixed at 3 mJ m^{-2} , perpendicular magnetic anisotropy (PMA) $K_u = 0.8 \times 10^6 \text{ J m}^{-3}$, the Gilbert damping coefficient $\alpha = 0.1$ and the value for the gyromagnetic constant γ is $1.67 \times 10^{11} \text{ rad T}^{-1} \text{ s}^{-1}$.^{7,28,49-51}

The skyrmion profile is assumed to be stable during motion due to the strong supporting DMI field. In the special case of a time-dependent steady state magnetization, the magnetization can be expressed as,^{52,53}

$$\vec{M} = \vec{M}(\vec{r} - \vec{r}(t)) \quad (14)$$

$$\frac{d\vec{M}}{dt} = \frac{\partial \vec{R}}{\partial t} \frac{\partial \vec{M}}{\partial \vec{R}} = \frac{\partial \vec{R}}{\partial t} \left(-\frac{\partial \vec{M}}{\partial \vec{r}} \right) = -(\vec{v} \cdot \nabla) \vec{M} \quad (15)$$

where \vec{v} is the steady state velocity. Substituting eqn (15) into the LLG equation yields the Thiele equation.

Conflicts of interest

There are no conflicts to declare.

Acknowledgements

The work was supported by the Singapore National Research Foundation, Prime Minister's Office under a Competitive Research Programme (Non-volatile Magnetic Logic and Memory Integrated Circuit Devices, NRF-CRP9-2011-01), and an Industry-IHL Partnership Program (NRF2015-IIP001-001). The support from an RIE2020 AME-Programmatic Grant (No. A1687b0033) is also acknowledged. WSL is also a member of the Singapore Spintronics Consortium (SG-SPIN).

References

- 1 I. Dzyaloshinsky, *J. Phys. Chem. Solids*, 1958, **4**, 241–255.

- 2 T. Moriya, *Phys. Rev. Lett.*, 1960, **4**, 228.
- 3 S. Heinze, K. Von Bergmann, M. Menzel, J. Brede, A. Kubetzka, R. Wiesendanger, G. Bihlmayer and S. Blügel, *Nat. Phys.*, 2011, **7**, 713–718.
- 4 A. Fert, V. Cros and J. Sampaio, *Nat. Nanotechnol.*, 2013, **8**, 152–156.
- 5 X. Zhang, M. Ezawa and Y. Zhou, *Sci. Rep.*, 2015, **5**, 9400.
- 6 F. Jonietz, S. Mühlbauer, C. Pfleiderer, A. Neubauer, W. Münzer, A. Bauer, T. Adams, R. Georgii, P. Böni and R. Duine, *Science*, 2010, **330**, 1648–1651.
- 7 J. Sampaio, V. Cros, S. Rohart, A. Thiaville and A. Fert, *Nat. Nanotechnol.*, 2013, **8**, 839–844.
- 8 I. Purnama, W. Gan, D. Wong and W. Lew, *Sci. Rep.*, 2015, **5**, 10620.
- 9 H. T. Fook, W. L. Gan, I. Purnama and W. S. Lew, *IEEE Trans. Magn.*, 2015, **51**, 1–4.
- 10 X. Yu, N. Kanazawa, W. Zhang, T. Nagai, T. Hara, K. Kimoto, Y. Matsui, Y. Onose and Y. Tokura, *Nat. Commun.*, 2012, **3**, 988.
- 11 H. T. Fook, W. L. Gan and W. S. Lew, *Sci. Rep.*, 2016, **6**, 21099.
- 12 S. Woo, K. Litzius, B. Krüger, M.-Y. Im, L. Caretta, K. Richter, M. Mann, A. Krone, R. M. Reeve and M. Weigand, *Nat. Mater.*, 2016, **15**, 501–506.
- 13 A. Hrabec, J. Sampaio, M. Belmeguenai, I. Gross, R. Weil, S. M. Chérif, A. Stashkevich, V. Jacques, A. Thiaville and S. Rohart, *Nat. Commun.*, 2016, arXiv:1611.00647.
- 14 O. Boule, J. Vogel, H. Yang, S. Pizzini, D. de Souza Chaves, A. Locatelli, T. O. Montes, A. Sala, L. D. Buda-Prejbeanu, O. Klein, M. Belmeguenai, Y. Roussigne, A. Stashkevich, S. M. Cherif, L. Aballe, M. Foerster, M. Chshiev, S. Auffret, I. M. Miron and G. Gaudin, *Nat. Nanotechnol.*, 2016, **11**, 449–454.
- 15 J. Kim, K.-J. Kim and S.-B. Choe, *IEEE Trans. Magn.*, 2009, **45**, 3909–3911.
- 16 K.-J. Kim, J.-C. Lee, S.-B. Choe and K.-H. Shin, *Appl. Phys. Lett.*, 2008, **92**, 192509.
- 17 A. Yamaguchi, S. Nasu, H. Tanigawa, T. Ono, K. Miyake, K. Mibu and T. Shinjo, *Appl. Phys. Lett.*, 2005, **86**, 012511.
- 18 S. Kanai, M. Yamanouchi, S. Ikeda, Y. Nakatani, F. Matsukura and H. Ohno, *Appl. Phys. Lett.*, 2012, **101**, 122403.
- 19 Y. Shiota, T. Nozaki, F. Bonell, S. Murakami, T. Shinjo and Y. Suzuki, *Nat. Mater.*, 2012, **11**, 39.
- 20 H. Kakizakai, K. Yamada, M. Kawaguchi, K. Shimamura, S. Fukami, N. Ishiwata, D. Chiba and T. Ono, *Jpn. J. Appl. Phys.*, 2013, **52**, 070206.
- 21 G. Yu, P. Upadhyaya, X. Li, W. Li, S. K. Kim, Y. Fan, K. L. Wong, Y. Tserkovnyak, P. K. Amiri and K. L. Wang, *Nano Lett.*, 2016, **16**, 1981–1988.
- 22 P.-J. Hsu, A. Kubetzka, A. Finco, N. Romming, K. von Bergmann and R. Wiesendanger, *Nat. Nanotechnol.*, 2017, **12**, 123–126.
- 23 D. Chiba, M. Sawicki, Y. Nishitani, Y. Nakatani, F. Matsukura and H. Ohno, *Nature*, 2008, **455**, 515.
- 24 T. Maruyama, Y. Shiota, T. Nozaki, K. Ohta, N. Toda, M. Mizuguchi, A. Tulapurkar, T. Shinjo, M. Shiraishi and S. Mizukami, *Nat. Nanotechnol.*, 2009, **4**, 158–161.
- 25 F. Ando, H. Kakizakai, T. Koyama, K. Yamada, M. Kawaguchi, S. Kim, K.-J. Kim, T. Moriyama, D. Chiba and T. Ono, *Appl. Phys. Lett.*, 2016, **109**, 022401.
- 26 H. Kakizakai, F. Ando, T. Koyama, K. Yamada, M. Kawaguchi, S. Kim, K.-J. Kim, T. Moriyama, D. Chiba and T. Ono, *Appl. Phys. Express*, 2016, **9**, 063004.
- 27 D. Chiba, M. Kawaguchi, S. Fukami, N. Ishiwata, K. Shimamura, K. Kobayashi and T. Ono, *Nat. Commun.*, 2012, **3**, 888.
- 28 W. Kang, Y. Huang, C. Zheng, W. Lv, N. Lei, Y. Zhang, X. Zhang, Y. Zhou and W. Zhao, *Sci. Rep.*, 2016, **6**, 23164.
- 29 J. Wang, J. Xia, X. Zhang, G. Zhao, J. Wu, Y. Xu, Z. Zou and Y. Zhou, 2017, arXiv preprint arXiv:1709.03733.
- 30 P. Upadhyaya, G. Yu, P. K. Amiri and K. L. Wang, *Phys. Rev. B: Condens. Matter Mater. Phys.*, 2015, **92**, 134411.
- 31 W. Kang, C. Zheng, Y. Huang, X. Zhang, Y. Zhou, W. Lv and W. Zhao, *IEEE Electron Device Lett.*, 2016, **37**, 924–927.
- 32 C. Navau, N. Del-Valle and A. Sanchez, *Phys. Rev. B*, 2016, **94**, 184104.
- 33 R. Wiesendanger, *Nat. Rev. Mater.*, 2016, **1**, 16044.
- 34 A. Soumyanarayanan, N. Reyren, A. Fert and C. Panagopoulos, 2016, arXiv preprint arXiv:1611.09521.
- 35 I. Makhfudz, B. Krüger and O. Tchernyshyov, *Phys. Rev. Lett.*, 2012, **109**, 217201.
- 36 N. Nagaosa and Y. Tokura, *Nat. Nanotechnol.*, 2013, **8**, 899–911.
- 37 K. Everschor-Sitte and M. Sitte, *J. Appl. Phys.*, 2014, **115**, 172602.
- 38 R. Tomasello, E. Martinez, R. Zivieri, L. Torres, M. Carpentieri and G. Finocchio, *Sci. Rep.*, 2014, **4**, 6784.
- 39 X. Zhang, Y. Zhou and M. Ezawa, *Nat. Commun.*, 2016, **7**, 10293.
- 40 W. Jiang, X. Zhang, G. Yu, W. Zhang, X. Wang, M. B. Jungfleisch, J. E. Pearson, X. Cheng, O. Heinonen and K. L. Wang, *Nat. Phys.*, 2017, **13**, 162–169.
- 41 K. Y. Guslienko, V. Novosad, Y. Otani, H. Shima and K. Fukamichi, *Phys. Rev. B: Condens. Matter Mater. Phys.*, 2001, **65**, 024414.
- 42 J. Iwasaki, M. Mochizuki and N. Nagaosa, *Nat. Nanotechnol.*, 2013, **8**, 742–747.
- 43 S. Rohart and A. Thiaville, *Phys. Rev. B: Condens. Matter Mater. Phys.*, 2013, **88**, 184422.
- 44 R. Skomski, H.-P. Oepen and J. Kirschner, *Phys. Rev. B: Condens. Matter Mater. Phys.*, 1998, **58**, 3223.
- 45 X. Zhang, G. Zhao, H. Fangohr, J. P. Liu, W. Xia, J. Xia and F. Morvan, *Sci. Rep.*, 2015, **5**, 9400.
- 46 A. Vansteenkiste, J. Leliaert, M. Dvornik, M. Helsen, F. Garcia-Sanchez and B. Van Waeyenberge, *AIP Adv.*, 2014, **4**, 107133.
- 47 E. Lifshitz and L. Pitaevskii, *Statistical physics*, Pergamon Press, Oxford, 1980.
- 48 A. Thiaville, Y. Nakatani, J. Miltat and Y. Suzuki, *EPL*, 2005, **69**, 990.
- 49 P. J. Metaxas, J. P. Jamet, A. Mougin, M. Cormier, J. Ferre, V. Baltz, B. Rodmacq, B. Dieny and R. L. Stamps, *Phys. Rev. Lett.*, 2007, **99**, 217208.

- 50 A. Barman, S. Wang, O. Hellwig, A. Berger, E. E. Fullerton and H. Schmidt, *J. Appl. Phys.*, 2007, **101**, 09D102.
- 51 A. Schellekens, L. Deen, D. Wang, J. Kohlhepp, H. Swagten and B. Koopmans, *Appl. Phys. Lett.*, 2013, **102**, 082405.
- 52 A. Thiele, *Phys. Rev. Lett.*, 1973, **30**, 230.
- 53 J. P. Liu, Z. Zhang and G. Zhao, *Skyrmions: Topological Structures, Properties, and Applications*, CRC Press, 2016.